Combustion and Flame 160 (2013) 861–869

Contents lists available at SciVerse ScienceDirect

Combustion and Flame

journal homepage: www.elsevier.com/locate/combustflame

Using Bayesian analysis to quantify uncertainties in the $H + O_2 \rightarrow OH + O$ reaction

Kenji Miki [a,*], Ernesto E. Prudencio [a], Sai Hung Cheung [a], Gabriel Terejanu [b]

[a] Institute for Computational Engineering and Sciences (ICES), The University of Texas at Austin, 1 University Station Austin, TX 78712, United States
[b] Department of Computer Science and Engineering, University of South Carolina, 315 Main St, Columbia, SC 29208

ARTICLE INFO

Article history:
Received 11 May 2012
Received in revised form 23 August 2012
Accepted 21 January 2013
Available online 26 February 2013

Keywords:
Bayesian approach
Stochastic system model
Uncertainty quantification
Arrhenius form
Irreducible uncertainty

ABSTRACT

A stochastic Bayesian approach is applied to investigate the uncertainty in the rate coefficient of $H + O_2 \rightarrow OH + O$ (k_1) using the latest shock-tube experimental data. We simultaneously calibrate all random variables using a recently developed stochastic simulation algorithm which allows for efficient sampling in the high-dimensional parameter space. We introduce the idea of "irreducible" uncertainty when considering other parameters in the system. Nine stochastic models are constructed depending on the choice of uncertainties, hydrogen concentration, gas temperature, pressure, and rate coefficients of other reactions. The sensitivity analysis of uncertainty in k_1 on these uncertainty parameters is performed. It is shown that the introduction of "irreducible" uncertainty does not always increase the uncertainty of k_1. In addition, we observe the high sensitivity of uncertainty in k_1 to the uncertainty in the measured time-shift. Our results show the strong temperature dependence of the uncertainty in the rate coefficient.

1. Introduction

At 7th International Conference on Chemical Kinetics (2011, MA), one whole session was dedicated to the uncertainty quantification (UQ) in terms of chemical kinetics. Their conclusions highlighted importance of making the comprehensive experimental database of the chemical kinetics and uncertainties associated with these experimental data.

About the data, there are two types of so-called "experimental" data: one is the "raw" data and the other is the "reduced" (i.e. post-processed) data. Typically, in the combustion experiments, the raw data is composed of the radiation traces, species concentration histories, etc. On the other hand, the "reduced" data is, for instance, the rate coefficients. Indeed, experimentalists construct a reduced kinetic mechanism based on their knowledge and assumptions, and then calibrate the rate coefficients in order to reasonably reproduce this "raw" data. In many literatures, both types of data mentioned are treated simply as "experimental" data. Due to the additional uncertainty associated with a reduction procedure, these two types of data have a different degree of uncertainty and we need to pay extra attention when using them in the same system. In fact, traditional procedures for validation of models in computational sciences and engineering are often related to data fitting in the sense that the closer the output quantities computed by models are to experimental observations, the better the models should be. It is clear that, for such processes, experimental data play a critical role, not only for the calibration of the model parameters (e.g. reaction rate constants, etc.), but also for the validation of the model itself. To this aim, it is important to understand the difference between the model uncertainty and the experimental uncertainty. When the "reduced" data is used, the experimental uncertainty have to be included the uncertainty related to the reduction procedure [1]. In the recent work of Turányi et al. [2], they proposed a new approach, in which they rigorously take into account both "raw" data and "reduced" data (called direct and indirect in their paper) during the calibration process.

The objective of this study is to perform a post-processing of the experimental ("raw") data and give a supplement to the uncertainty of the "reduced" data. To this aim, we propose the comprehensive and robust calibration process based on Bayesian approach. In order to assess the capability of our analysis, we utilize the proposed methodology to investigate the uncertainty in the rate coefficient of $H + O_2 \rightarrow OH + O$. The well-calibrated "raw" experimental data recently acquired at the High Temperature Gasdynamics Laboratory at Stanford University [3] was available, describing the ignition phenomena of $O_2/H_2/Ar$ mixture behind the reflected shock waves. There are numerous studies conducted to compute this rate coefficient (see the NIST database [4]), however a large scatter of the coefficients in the Arrhenius form is still present (see Table 1), which we attribute to the drawback during the conventional calibration procedure, as well as to the difficulty of the experiments.

There are many other noticeable UQ works in the chemical kinetic field. For instance, Sheen et al. [5] developed the spectral expansion technique and performed the kinetic uncertainty

* Corresponding author. Tel.: +1 404 421 2301.
E-mail address: kenji@ices.utexas.edu (K. Miki).

0010-2180/$ - see front matter © 2013 The Combustion Institute. Published by Elsevier Inc. All rights reserved.
http://dx.doi.org/10.1016/j.combustflame.2013.01.020

Table 1
Results of Arrhenius coefficients of $H + O_2 \rightarrow OH + O$ in the selected past studies [4]. (*Note*: Turányi et al. provided the temperature-dependent uncertainty in k_1. See [2].)

Reference	T (K)	A_1 ($cm^3\ mol^{-1}\ s^{-1}$)	m_1	Θ_1 (K)
Experimental works				
Hong et al. [3]	1100 – 3370	$(1.04 \pm 0.03) \times 10^{14}$	0.0	7705 ± 40
Yuan et al. [27]	1050 – 2700	1.59×10^{17}	−0.93	8490
Pirraglia et al. [23]	962 – 1700	$(1.68 \pm 0.19) \times 10^{14}$	0.0	8119 ± 139
Fujii and Shin [28]	1900 – 2650	5.97×10^{14}	0.0	11400
Frank and Just [29]	1700 – 2500	$(2.43 \pm 0.33) \times 10^{14}$	0.0	8700 ± 261
Namoradze et al. [30]	839 – 924	9.72×10^{12}	0.0	6369
Theoretical works				
Miller and Garrett [31]	1000 – 5500	6.69×10^{11}	0.55	5970
Germann and Miller [32]	500 – 2000	1.76×10^{14}	0.0	8381
Post-processing works				
Turányi [2]	980 – 2000	1.88×10^{11}	−0.0957	7515

propagation through the ethylene combustion and recently extended the model [6]. Russi et al. [7] utilized the Data Collaboration method [8] and took into account the uncertainty in experimental observations and model parameters in the context of sensitivity analysis. Also, recently Nagy and Turányi [9] investigated the uncertainties associated with the expression of the rate coefficient in the Arrhenius form and emphasized the importance of considering the correlation among the Arrhenius coefficients in the varying temperature chemical kinetic systems. Recently, Turányi et al. [2] further extended their model to consider the covariance matrix during minimizing the objective function so that it is possible to capture the structure of the uncertainties. In addition, uncertainty analysis solving an inverse problem with the help of Bayesian approach can be also seen in literature (e.g. [10–12]).

In this paper, we discuss a new type of uncertainty analysis using Bayesian approach and take into account the effects of uncertainties on some parameters in the model, such as gas temperature. Indeed, it might not be a good idea to specify these parameters deterministically, but we should treat them instead as "incompletely known" and consider the effect of their uncertainties on the model behavior. Here, we call these extra uncertainties as "irreducible" uncertainties. For example, the uncertainties of other rate coefficients from the literature can also be categorized into this type of uncertainty. The novel feature of the method used in this paper is that we solve the inverse problem in the context of uncertain inputs, such as temperature and pressure. The uncertainty in the inputs arises due to the noise introduced by the measurement apparatus. These input variables are not under calibration. The objective of model calibration is to quantify the uncertainty in the rate coefficient, k_1, by accounting for the uncertainty in the inputs. There are many studies dealing with how to properly propagate this type of uncertainty in forward propagations, but few of them address it in the context of inverse propagations.

The paper is organized as follows: in the next section, we present the proposed UQ model and highlight the difference from the conventional calibration procedure. The brief descriptions of the physical model and the experimental data are provided in Section 4. In Section 4, the stochastic model is constructed based on our past studies [13], and the summary of the different stochastic models with the different choices of random model parameters is provided. In the result section, a detailed comparison of the results obtained using different models and statistical dependence (i.e., sensitivity analysis) between the "irreducible" uncertainties and the uncertainty in the rate coefficient is provided.

2. The proposed calibration methodology

Figure 1 schematically shows the proposed calibration methodology based on Bayesian approach. Let $\mathcal{M}_i$ designate a i^{th} stochastic system model class [14,15]. Each stochastic system model in $\mathcal{M}_i$ is specified by uncertain model parameters $\boldsymbol{\theta} \in \Omega \subset \mathbb{R}^d$. One can use data $\boldsymbol{D}$ to compute the posterior probability density function (PDF) $p(\boldsymbol{\theta}|\boldsymbol{D}, \mathcal{M}_i)$ in the Bayes' theorem,

$$p(\boldsymbol{\theta}|\boldsymbol{D}, \mathcal{M}_i) = \frac{p(\boldsymbol{D}|\boldsymbol{\theta}, \mathcal{M}_i)p(\boldsymbol{\theta}|\mathcal{M}_i)}{c}, \tag{1}$$

where c is a normalizing constant that makes the probability volume under the posterior PDF equal to unity, $p(\boldsymbol{D}|\boldsymbol{\theta}, \mathcal{M}_i)$ is the likelihood function, and $p(\boldsymbol{\theta}|\mathcal{M}_i)$ is the prior PDF for $\boldsymbol{\theta}$. The likelihood function expresses the probability of observing $\boldsymbol{D}$ based on the model $\boldsymbol{\theta}$ in the model class $\mathcal{M}_i$, and is commonly chosen to have the form

$$p(\boldsymbol{D}|\boldsymbol{\theta}, \mathcal{M}_i) = \frac{1}{\sqrt{2\pi|\Gamma|}} \exp\left\{-\frac{1}{2}(\boldsymbol{D} - \boldsymbol{X})^T \Gamma^{-1} (\boldsymbol{D} - \boldsymbol{X})\right\}, \tag{2}$$

where $\boldsymbol{X} \in \mathbb{R}^{N_d}$ is the computed model output, $\Gamma \in \mathbb{R}^{N_d \times N_d}$ is a *covariance matrix*, which still needs to be specified, and N_d indicates the number of data points. Here, errors at all data points are assumed to be statistically independent of each other, in other words that Γ is a diagonal matrix: $\Gamma_{ij} = \sigma^2 \delta_{ij}$. Here, σ^2 ppm is unknown variance which is the sum of the experimental errors (σ^2_{exp} ppm) and the modeling errors (σ^2_p ppm). When the same experimental data is used for all $\boldsymbol{\mathcal{M}}$, the calibration of σ^2 ppm will provide an indication of the modeling error σ^2_p ppm.

The above calculation of the $p(\boldsymbol{\theta}|\boldsymbol{D}, \mathcal{M}_i)$ is called "inverse problem" (inside the dashed box in Fig. 1). One of the another important objectives of performing the above analysis is to make robust predictions about quantities of interest (QoI). This process is called "forward problem". Based on a candidate model class $\mathcal{M}_i$, all the probabilistic information for the prediction of a vector of QoI $\mathbf{Q}$ is contained in the posterior predictive PDF for $\mathbf{Q}$ given by the theorem of total probability:

$$p(\mathbf{Q}|\boldsymbol{D}, \mathcal{M}_i) = \int p(\mathbf{Q}|\boldsymbol{\theta}, \boldsymbol{D}, \mathcal{M}_i) \cdot p(\boldsymbol{\theta}|\boldsymbol{D}, \mathcal{M}_i) d\boldsymbol{\theta} \tag{3}$$

The above equation obtains the prediction $p(\mathbf{Q}|\boldsymbol{D}, \mathcal{M}_i)$ of a vector of QoI $\mathbf{Q} \in \mathbb{R}^q$ by summing up the prediction $p(\mathbf{Q}|\boldsymbol{\theta}, \boldsymbol{D}, \mathcal{M}_i)$ of each model specified by $\boldsymbol{\theta} \in \Omega$ weighted by its posterior probability $p(\boldsymbol{\theta}|\boldsymbol{D}, \mathcal{M}_i)d\boldsymbol{\theta}$. In this paper QoI is the rate coefficient k_1 of the reaction $H + O_2 \rightarrow OH + O$, with k_1 following the Arrhenius form: $k_1 = A_1 T^{m_1} \exp(-\Theta_1/T)$.

The prior PDFs, $p(\boldsymbol{\theta}|\mathcal{M}_i)$, are chosen as uniform distributions for A_1, m_1, Θ_1 and σ: U[10^{13},10^{28}] for A_1, U[−5,5] for m_1, U[0,20,000] for Θ_1, and U[0,1,000] for σ (Table 2). A large interval is assigned to the prior of A_1 due to possible nonzero values for m_1. Our prior PDFs cover all reported values [4,16]. We have adopted such broad uniform priors due to the large variation in the values reported in the literature. It should also be noted that, in the proposed Bayesian approach it is the posterior PDF, not the prior PDF, which ulti-

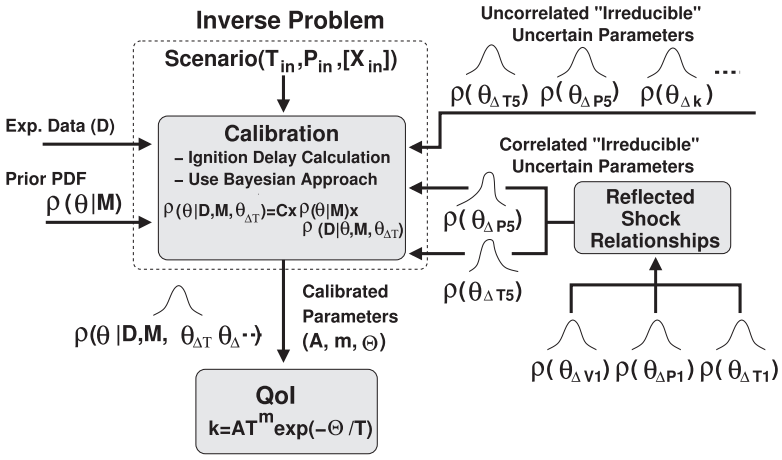

Fig. 1. Schematic of the proposed calibration procedure.

Table 2
Prior distribution for the model parameters of the rate coefficients. The intervals for the uniform priors are chosen based on past studies [4].

$p(A_1\|\mathcal{M}_i)$	$p(m_1\|\mathcal{M}_i)$	$p(\Theta_1\|\mathcal{M}_i)$	$p(\sigma\|\mathcal{M}_i)$
$U[10^{13},10^{28}]$	$U[-5,5]$	$U[0,20{,}000]$	$U[0,1000]$

mately quantifies the uncertainty of the model parameters by updating the prior distribution. Making use of the data, the proposed Bayesian approach will automatically assign low probability to the region of the model parameters (as encapsulated in the posterior PDF) that lead to poor agreement of the model with the data (less probable model).

On the right side of Fig. 1, another inputs, "irreducible" uncertain parameters, are introduced in the form of the probability functions. When we consider the "irreducible" uncertainty, the above expression of the likelihood function needs to be modified. Here, we assume that the uncertainty follows the Gaussian distribution denoted by $p(\mathbf{v}|\mathcal{M}_i,\boldsymbol{\theta}_{\boldsymbol{v}})$, where $\mathbf{v}$ is a vector storing "irreducible" uncertain parameters and $\boldsymbol{\theta}_{\boldsymbol{v}}$ is another vector storing parameters characterizing this distribution, such as mean and variance. Then, the resultant likelihood function needs to be averaged as follows:

$$p(\boldsymbol{D}|\mathcal{M}_i,\boldsymbol{\theta},\boldsymbol{\theta}_{\boldsymbol{v}}) = \int p(\boldsymbol{D}|\mathcal{M}_i,\boldsymbol{\theta},\mathbf{v})p(\mathbf{v}|\mathcal{M}_i,\boldsymbol{\theta}_{\boldsymbol{v}})d\mathbf{v} \tag{4}$$

This integration is not trivial, and it is computationally expensive if we approximate it by using the Monte Carlo method. In this study, we utilize the method recently developed and presented in [17].

3. Physical model and experimental data

Assuming that the temperature and pressure are constant during the reaction behind the reflected shock waves [3], the chemical reactions can be expressed in ordinary differential equations for each species. The forward rate coefficient of the rth reaction, $k_{f,r}$, is calculated using the modified Arrhenius equation: $k_{f,r} = A_r T^{m_r} \exp\left(-\frac{\Theta_r}{T}\right), r = 1,\ldots,N_r = 35$, where A_r and m_r are the pre-exponential Arrhenius parameters and Θ_r is the characteristic temperature of the activation energy. The corresponding backward rate coefficient, $k_{b,r}$, is obtained by $k_{b,r} = k_{f,r}/K_{C,r}$ where $K_{C,r}$ is the equilibrium constant determined by the thermochemical database [18]. We use the detailed chemical kinetic mechanism previously verified in [3] to model the H_2O profile behind the reflected shock wave. This mechanism considers 35 elementary reactions and nine species, O, H, H_2, O_2, OH, H_2O, HO_2, H_2O_2 and Ar.

The experimental data used in this paper was recently collected at the High Temperature Gasdynamics Laboratory at Stanford University [3]. The data is composed of six profiles of the H_2O concentration history behind the reflected shock waves over the temperature range 1100–1472 K. The detailed description of the shock tube experiment is provided in [19]. The significance of these measurements is that the temperature and pressure remain nearly constant for a relatively long time (~ms) in the mixture behind the reflected shock waves. Moreover, very careful calibration of the measurements was performed in the laboratory, and the experimental uncertainty for concentration measurements was relatively small. Table 4 shows six experimental scenarios composed of the gas temperature, T_5 K, pressure, P_5 atm, and percentage concentrations of H_2 and O_2 behind the shock waves. Note that the reason why we selected these six profiles is because it is necessary to avoid using redundant information, which results in underestimation of the uncertainties [20]. Besides, these data appear to have a sufficient information for estimating four unknown parameters. Ref. [19] reported uncertainties of $2\sigma_{T_5} = 10.2$ K for the low (1000 K) temperature measurements and $2\sigma_{T_5} = 9.4$ K for the high (1472 K) temperature measurements, as well as an uncertainty of less than 1% in the gas composition.

4. Description of stochastic models

Table 3 summarizes the calibrating parameters and the irreducible uncertain parameters. In this study, we consider nine models: $\mathcal{M}_i, i = 1,\ldots,9$. For model $\mathcal{M}_1$ and model $\mathcal{M}_2$, we perform the parameter calibrations without considering any irreducible uncertainties. (for the rest of study, model $\mathcal{M}_1$ is treated as a base case). The numbers of the calibration parameters are 4 ($\boldsymbol{\theta} = (A_1, m_1, \Theta_1, \sigma)$) for model $\mathcal{M}_1$ and 10 ($\boldsymbol{\theta} = (A_1, m_1, \Theta_1, \sigma, [H]_i : i = 1,\ldots,6)$) for model $\mathcal{M}_2$. In model $\mathcal{M}_2$, the initial impurities of H in the gas are considered. Note Hong et al. [3] considered the small amount of H atom in the gas to obtain the best fit to the data. Here, one of the objectives is to check if there is any temperature dependence of the posterior PDFs of H atom concentrations. In the rest of the models, we consider $\boldsymbol{\theta} = (A_1, m_1, \Theta_1, \sigma)$ and the irreducible uncertainties, $\boldsymbol{\theta}_{\boldsymbol{v}}$, related to the measurement time shift ($\mathcal{M}_3$), gas temperature/pressure ($\mathcal{M}_4$–$\mathcal{M}_7$), and the other rate coefficients ($\mathcal{M}_8$ and $\mathcal{M}_9$). The measurement time shift (denoted to Δt_s) may be a critical factor to bring additional uncertainties in the calibration process (Dr. D.E. Davidson, personal communication, July, 2011). We perform a parametric study to investigate how the level of the uncertainty in Δt_s affects the uncertainty in the rate coefficient k_1. We test four cases where we assign a Gaussian distribution with zero mean and

Table 3
Summary of the stochastic models.

	Calibrating param.					Irreducible uncertain param.							
Model	A_1	m_1	Θ_1	σ	$[H]_i$	Δt_s	T_5	P_5	T_1	P_1	V_1	k_{24}	k_{22}
$\mathcal{M}_1$	✓	✓	✓	✓	–	–	–	–	–	–	–	–	–
$\mathcal{M}_2$	✓	✓	✓	✓	✓	–	–	–	–	–	–	–	–
$\mathcal{M}_3$	✓	✓	✓	✓	–	✓	–	–	–	–	–	–	–
$\mathcal{M}_4$	✓	✓	✓	✓	–	–	✓	–	–	–	–	–	–
$\mathcal{M}_5$	✓	✓	✓	✓	–	–	–	✓	–	–	–	–	–
$\mathcal{M}_6$	✓	✓	✓	✓	–	–	✓	✓	–	–	–	–	–
$\mathcal{M}_7$	✓	✓	✓	✓	–	–	–	–	✓	✓	✓	–	–
$\mathcal{M}_8$	✓	✓	✓	✓	–	–	–	–	✓	✓	✓	✓	–
$\mathcal{M}_9$	✓	✓	✓	✓	–	–	–	–	✓	✓	✓	✓	✓

Table 4
Experimental scenarios (O_2/H_2/Ar mixture) [3].

Index	T_5 (K)	P_5 (atm)	$[H_2]$ (%)	$[O_2]$ (%)
D_1	1100	1.95	2.90	0.10
D_2	1197	1.84	2.90	0.10
D_3	1256	2.01	2.90	0.10
D_4	1317	1.91	0.90	0.10
D_5	1448	1.85	0.90	0.10
D_6	1472	1.83	0.90	0.10

the variance equal to $\sigma_{\Delta t_s} = 5$ μs, 10 μs, 20 μs, and 50 μs. For model $\mathcal{M}_4$, we consider the post-shock gas temperature (T_5) as irreducible uncertainty. Based on the reported uncertainty of T_5 by Hong et al., σ_{T_5} is set to 5 K. Similarly, model $\mathcal{M}_5$ considers the post-shock gas pressure uncertainty that is σ_{P_5} equal to 0.01 atm. Then, model $\mathcal{M}_6$ takes account of both of them at the same time. In this case, we input two Gaussian distributions of σ_{T_5} and σ_{P_5} without considering the correlation among them. We call these parameters "uncorrelated" irreducible uncertainty parameters (see the top right corner of Fig. 1). However, in reality, T_5 and P_5 are strongly correlated and can be expressed by the well-known ideal shock relations, which are the functions of the incident shock gas temperature, T_1, velocity V_1 (or Mach number), and pressure P_1. Therefore, it is more reasonable to consider the uncertainties of T_1, V_1, and P_1, and then to propagate these uncertainties through the T_5 and P_5. In this case, the resulting PDFs of T_5 and P_5 are no more Gaussian distributions and correlated to each other (see the bottom right corner of Fig. 1). The uncertainties of T_1, V_1, and P_1 are set to $\sigma_{T_1} = 0.15$ K, $\sigma_{V_1} = 1.89 \times 10^{-3}$ km/s, and $\sigma_{P_1} = 3.29 \times 10^{-5}$ atom, respectively [21]. These uncertainties give the same values for σ_{T_5} and σ_{P_5}. The detailed uncertainty analysis for the calculated ideal shock conditions immediately behind the reflected shock wave is provided at Appendix C in [21]. Finally, the uncertainties of other rate coefficients are considered "uncorrelated" irreducible uncertainty parameters. Based on the sensitivity analysis [3], we consider the uncertainty of the rate coefficient of $H + HO_2 \rightarrow H_2 + O_2$ (k_{24}) in $\mathcal{M}_8$ and set $\sigma_{k_{24}}$ to 0.1 [16], which is expressed by log k. $\mathcal{M}_9$ additionally considers the uncertainty of the rate coefficient of $H + HO_2 \rightarrow 2OH$ (k_{22}), and $\sigma_{k_{22}}$ is assigned to be 0.05 [16]. In this case, the random variables associated with the irreducible uncertainties are $\boldsymbol{\theta_v} = (T_1, P_1, V_1, k_{24}, k_{22})$, which requires solving the five-dimensional integration (see Eq. (4)). Significance of the proposed methodology here is to take into account these uncertainties in a mathematically consistent manner when solving the inverse problem. Therefore, these uncertainties rigorously propagate through the estimation of the uncertainty of QoIs.

5. Results and discussion

In the numerical experiments shown below, the posterior PDFs are sampled with the Markov Chain Monte Carlo method proposed in [17]. For the calibration process we use up to 120,000 samples to sweep the parameter spaces. Each whole calibration-prediction process took less than 4 h on a modern serial Linux machine thanks to the simplicity of the model. The current numerical methodology is very efficient and feasible for various engineering applications (e.g. [17,22,11,1]).

5.1. Calibration using the manufactured data

Before using actual experimental data, we verify that the proposed inversion methodology works properly. In order to do so, we use the physico-mathematical model to generate data by setting the model parameters to their nominal values. Gaussian noise is further inserted in the computed values. These data sets will be referred to as "manufactured data" in the following. In this exercise, we test the case using model $\mathcal{M}_2$. We assume that the initial H concentrations decrease as the gas temperature increases. Figure 2 shows the experimental data (D_1) from [3] and the manifactured data. Due to our assumption that σ^2 is not a time dependent variable and an additive error is likely to represent the current problem, the 95% confidence interval (CI) is bounded by two solid lines. Note that it is not realistic to presume that the uncertainties in the measured H_2O concentration in regions A (pre-ignition zone) and C (post-ignition zone) are at the same level as for the measurements within B [13]. We use the data only in region B where the gradient of the profile is approximately constant. Figure 3 shows the posterior PDFs of the model parameters of $\mathcal{M}_2$. We are able to retrieve the nominal values indicated by the dashed lines. Indeed, the data inform well enough Arrhenius parameters as well as H concentrations in the sense that the resulting PDFs have small variances. Therefore, we may conclude that the inverse problem is

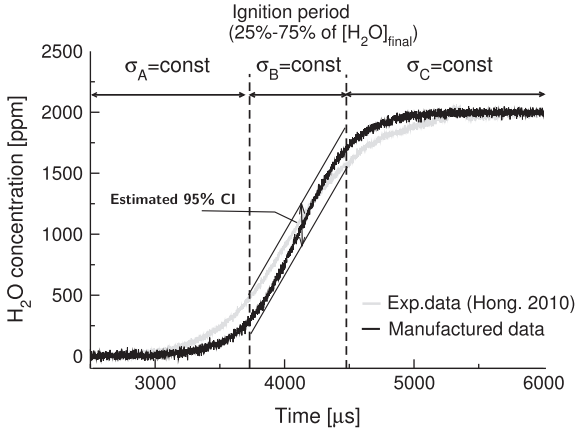

Fig. 2. Experimental data from [3] and manufactured data. The solid lines represent the 95% CI.

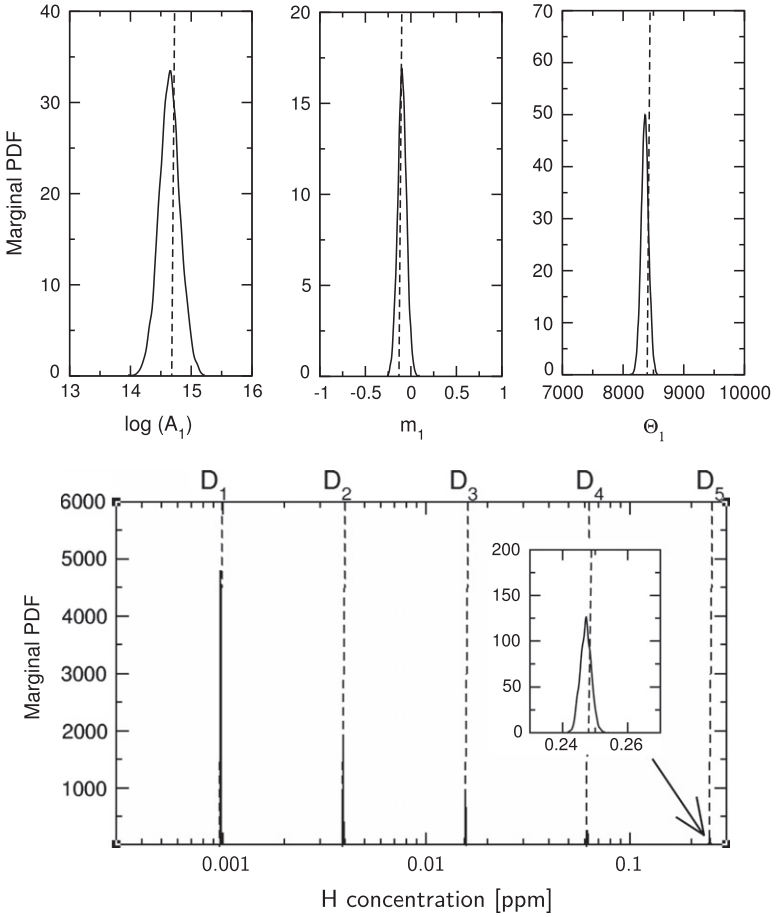

Fig. 3. Posterior PDFs of the model parameters: (top left) log (A_1), (top middle) m_1, (top right) Θ_1, and (bottom) H concentrations.

correctly posed and that one should be able to identify the model parameters.

5.2. Calibration with the experimental data [3]

Figure 4 shows (top) the predicted 95% CI of k_1 when using model $\mathcal{M}_1$, as well as the experimental data from [23,24] and the reference curve fits from [3,25], and (bottom) the percentage uncertainty in k_1 calculated based on two standard deviations and the reported uncertainties (boxes) at $T = 1500$ K and 1100 K [3]. The computed k_1 agrees well with the value reported in [3] and the experimental data within the experimental temperature range used for calibration. However, the uncertainty is significantly underestimated within the temperature range of the available experimental data and increases in the high temperature region ($T > 2000$ K). The reason why we underestimate the uncertainty is related to the problem of this simple calibration procedure (the detailed discussion about this issue is provided in our previous study [13]) Note that even when we introduce more unknown random variables subject to calibration (like model $\mathcal{M}_2$), this problem is not resolved. This motivates us to perform the rest of study in order to understand the importance of "irreducible" uncertainties. On the other hand, the increase of uncertainty in the high temperature region is related to the problematic nature of "extrapolation" of k_1 in the high temperature regions using the calibrated model (1100–1470 K).

Figure 5 shows the predicted 95% CI when using model $\mathcal{M}_2$. We observe that H concentration significantly increases as the gas temperature increases. This may be due to the remaining of H atom

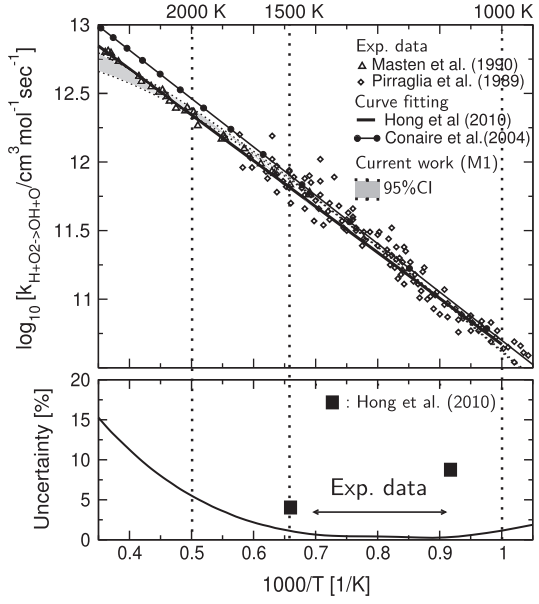

Fig. 4. (top) 95% CI for log (k_1) against 1000/T 1/K, the experimental data from [23,24] and the reference curve fits from [3,25], and (bottom) percentage uncertainty in k_1 based on two standard deviations against 1000/T 1/K.

from the previous experiments or possible vapor of H_2O in the shock-tube. Indeed, Hong et al. reported that the amount of H atom artificially added during Lutz et al. [26] calculation exponentially decreases as the gas temperature drops. In their calculation, they

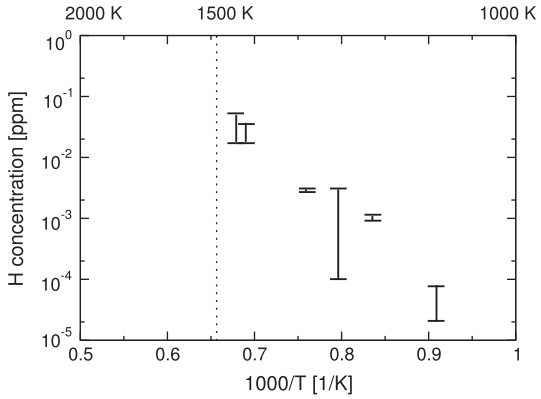

Fig. 5. 95% CI for H concentration against 1000/*T* 1/*K*.

considered 0.0012 ppm of H atoms to get a better agreement with the data D_1. The calculated uncertainty of k_1 is almost the same as the one shown in Fig. 4(bottom). The increase of calibrating parameter does not change the degree of uncertainty of k_1 (not shown).

Next, we consider the uncertainty of the measured time-shift and introduce it as "irreducible" uncertainty. There is no *a priori* information about the degree of this uncertainty. Thus, we perform parametric study of the measured time-shift and considered four different values: $\sigma_{\Delta t_s} = 5\ \mu s$, $10\ \mu s$, $20\ \mu s$, and $50\ \mu s$. Figure 6 shows the percentage uncertainty in k_1 against $\sigma_{\Delta t_s}$ at four different temperature, 1000 K (•), 1500 K (□), 2000 K (♦), and 2500 K (△). The dashed lines are the reported uncertainty computed deterministically in [3]. Compared with the result using model $\mathcal{M}_1$ equivalent to the case $\sigma_{\Delta t_s} = 0\ \mu s$, the degree of uncertainties significantly increases. Only 5 μs uncertainty in the measured time-shift results in about 6% and 16% uncertainties at $T = 1000$ K and 2500 K, respectively. The uncertainty monotonically increases as the $\sigma_{\Delta t_s}$ increases. In this model, the reported uncertainties are much closer to the calculated uncertainty. It is worth mentioning that the reason why •s and □s are similar is because we have the experimental data in this temperature range. This parametric study shows high sensitivity of uncertainty of k_1 to $\sigma_{\Delta t_s}$.

In the next set of experiments, we introduce the uncertainty of the gas temperature (T_5) and pressure (P_5) as "irreducible" uncertainty. As previously explained, these two quantities are correlated through the inflow scenarios: T_1, P_1 and V_1. For a fair comparison among the results using $\mathcal{M}_4, \mathcal{M}_5, \mathcal{M}_6$ and $\mathcal{M}_7$, we make sure that the "correlated" PDFs of T_5 and P_5 have the similar variances to the "uncorrelated" PDFs of T_5 and P_5. Figure 7 shows the resulting correlated PDFs of T_5 and P_5 solving the reflected shock relationships with the input of the uncorrelated PDFs of T_1, P_1, and V_1. Even though the variance of T_5 at $T = 1500$ K is slightly larger than the one at $T = 1000$ K, the result is satisfactory. Figure 8 shows the predicted 95% CI of k_1 using (a) $\mathcal{M}_4$, (b) $\mathcal{M}_5$, (c) $\mathcal{M}_6$, and $\mathcal{M}_7$, and the experimental data from [23,24]. For all models, the predicted log k_1 agrees with the experimental data within the temperature range of the data used in this study (1100–1472 K) even though these data are "reduced" data, not "raw" data. Also, note there are also other factors that affects the predictions such as model error included in this study. When we consider only the uncertainty of gas temperature as "irreducible" uncertainty, the gradient of log k_1 becomes steeper compared with the case of $\mathcal{M}_1$ (see Fig. 4) and as a result, the discrepancy from the data becomes large in the high temperature region. On the other hand, Fig. 8b ($\mathcal{M}_5$) shows the excellent agreement with the data within the entire temperature range. It is interesting that the predicted uncertainties for both case are smaller in the high temperature region (above 1700 K) than the one obtained by model $\mathcal{M}_1$, which is shown later in Fig. 10. This will be discussed later in detail. In Fig. 8c and d, we observe that the calculated uncertainties are much larger when compared to Fig. 8a and b, and that there is negligible difference between these two profiles. The combination of these two "irreducible" uncertainties significantly enhances the uncertainty of k_1 due to more freedom in statistical dependence among the parameters. On the other hand, to consider the correlation between T_5 and P_5 has a negligible impact on the prediction of uncertainty in k_1. The resulting marginal posterior PDFs of the Arrhenius coefficients are shown in Fig. 9. We observe that there is a great agreement between the PDFs from model $\mathcal{M}_6$ and model $\mathcal{M}_7$ and that the variance in these PDFs remains larger than in the ones obtained by model $\mathcal{M}_4$ and model $\mathcal{M}_5$. Considering the small uncertainty in k_1, the calculated large variance in the PDFs could seem surprising. However, multiple combinations of three parameters result in similar values of k_1, i.e., they are strongly correlated with each other. A non-zero value of m_1 shown in Fig. 9b results in the large variation of A_1. Also, the predicted Θ_1 varies from 7000 K to 11,000 K. We conclude that it is difficult to capture the temperature dependence of k_1 using the current data, especially when considering multiple "irreducible" uncertainties.

Fig. 10 shows the percentage uncertainty estimated by models $\mathcal{M}_4$–$\mathcal{M}_9$ and model $\mathcal{M}_1$ when not considering any "irreducible" uncertainties. We observe significant increase of uncertainties within the temperature range available for the calibration data when considering the "irreducible" uncertainties except model $\mathcal{M}_5$. The overly underestimated uncertainty by model $\mathcal{M}_5$ is surprising. This means that the uncertainty of pressure let the model

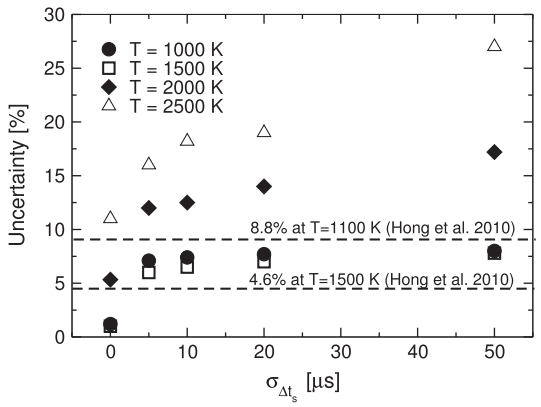

Fig. 6. Percentage uncertainty in k_1 based on two standard deviations against the uncertainty of the measured time-shift, $\sigma_{\Delta t_s}$.

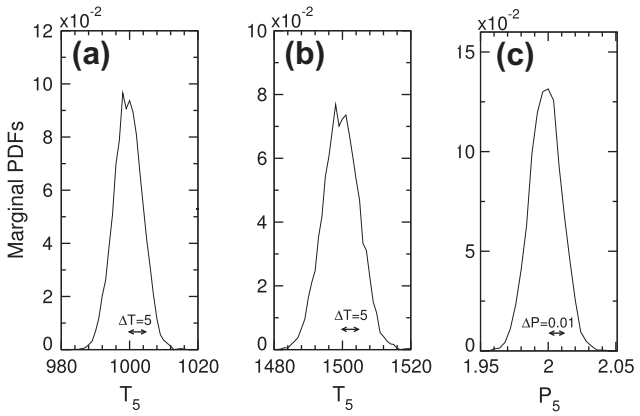

Fig. 7. PDFs of T_5 and P_5 calculated by the reflected shock relationships. The input PDFs of T_1, P_1 and V_1 are based on the report [21].

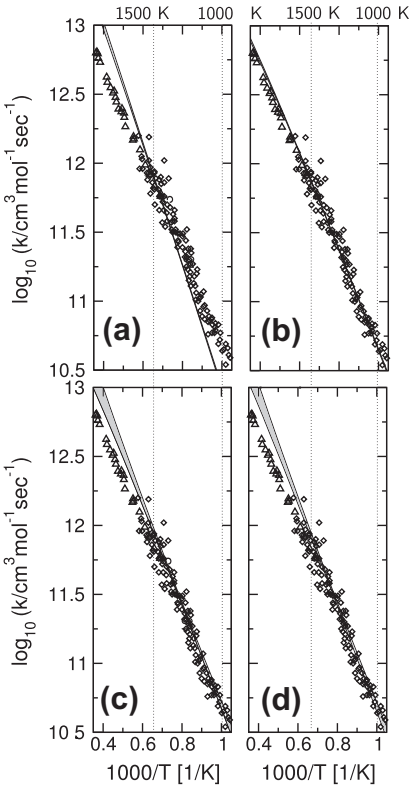

Fig. 8. 95% CI for log (k_1) against 1000/T 1/K and the experimental data from [23,24], (a) $\mathcal{M}_4$, (b) $\mathcal{M}_5$, (c) $\mathcal{M}_6$, and (d) $\mathcal{M}_7$.

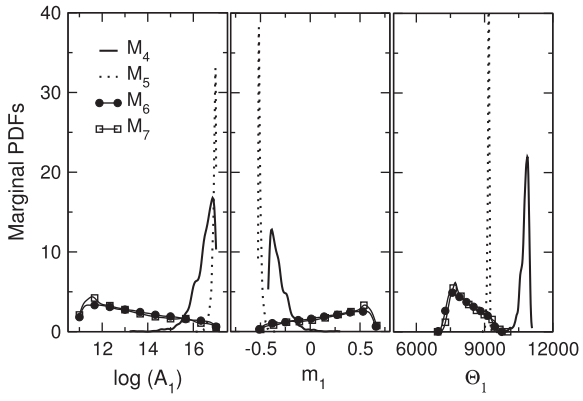

Fig. 9. Posterior PDFs of A_1, m_1, Θ_1 for models $\mathcal{M}_4$–$\mathcal{M}_7$.

fit the data well without any adjustment of k_1. On the other hand, the introduction of the temperature uncertainty increases the uncertainty in k_1, ~4% at 2000 K, and ~2% at 1500 K. However, this is still much less than the reported uncertainty (±4.6% at 1500 K [3]). When we consider both the temperature and pressure uncertainties ($\mathcal{M}_6$ and $\mathcal{M}_7$), we observe the uncertainty significantly increases – i.e., ~11% at 2000 K, ±4.2% at 1500 K, and ±7% at 1000 K), which are much closer to the reported values [3]. Also, in these cases, the uncertainty is appreciable even within the temperature range of the available experimental data. However, when we take into account the uncertainties from the rate coefficients of the other reactions, $H + HO_2 \rightarrow H_2 + O_2$ (k_{24}) and $H + HO_2 \rightarrow 2OH$ (k_{22}), the predicted uncertainties drops. To understand this, the marginal posterior PDFs of σ^2 are shown in Fig. 11. $\mathcal{M}_1$ shows the largest value of σ^2 (~200 ppm). We observe that the introduction of any kind of "irreducible" uncertainties reduces σ^2. It is surprising that the small amount of uncertainty of temperature significantly reduces σ^2, in other words, the difference between the data and the model outputs may be strongly related to the gas temperature uncertainty. On the other hand, when compared to other cases ($\mathcal{M}_4$–$\mathcal{M}_7$), $\mathcal{M}_8$ and $\mathcal{M}_9$ have relatively large values of σ^2. The increase of σ^2 compensates the reduction of uncertainty in k_1, which is smaller than the one predicted by $\mathcal{M}_6$ (or $\mathcal{M}_7$).

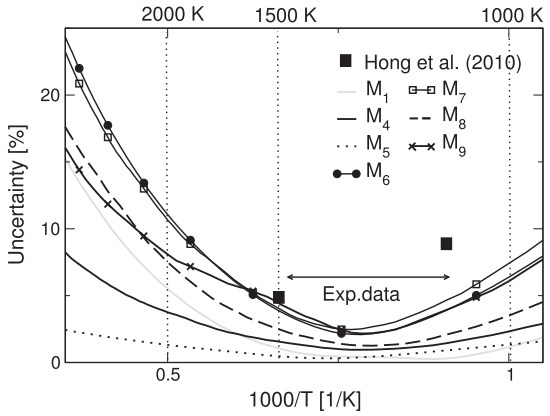

Fig. 10. Percentage uncertainty in k_1 based on two standard deviations against 1000/T 1/K.

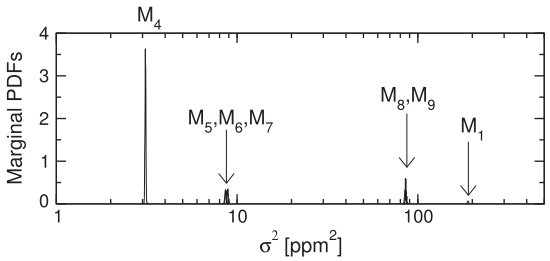

Fig. 11. Posterior PDFs of σ^2 for models $\mathcal{M}_1$, and $\mathcal{M}_4$–$\mathcal{M}_9$.

From this exercise, we can see the complex stochastic dependence of the uncertainties of k_1 on the total modeling error, experimental error, as well as "irreducible" uncertainties. It is worth emphasizing that the introduction of "irreducible" uncertainties does not always increase the uncertainty in k_1. In the recent works of Panesi et al. [1], the comprehensive uncertainty analysis for k_1 was performed and the temperature-dependent uncertainty, which is characterized by the uncertainty factor, f, defined as $f = \log_{10}\left(k_1(T)/k_1^{min}(T)\right) = \log_{10}(k_1^{max}(T)/k_1(T))$, was provided. Combining all available data (i.e., raw and reduced data), they obtained $f \sim 0.2$ at 900 K, $f \sim 0.14$ at 1500 K, and $f \sim 0.2$ at 2700 K based on 2σ. It is misleading to directly compare our results with theirs since our uncertainty estimation are provided only for the data used in this analysis. However, it is interesting to see that their study also shows the increase of uncertainty in k_1 in the high temperature region.

Finally, Fig. 12 shows the sensitivity analysis of the effect of the "irreducible" uncertainties on the uncertainty in k_1 at three different temperatures: (a) 1000 K, (b) 1500 K, and (c) 2000 K. For instance, based on the uncertainty calculated by model $\mathcal{M}_1$, there is ~6% increase in uncertainty at $T = 1000$ K when introducing the measured time-shift: $\sigma_{\Delta t_s} = 5$ μs. In general, we observe that the absolute magnitude of uncertainties increases as the gas temperature increases. Considering that the temperature range of the data used in this study is 1100–1472 K, the "extrapolation" of k_1 in the high temperature region using the calibrated model causes the mode to be less constrained (i.e., more uncertain). The main

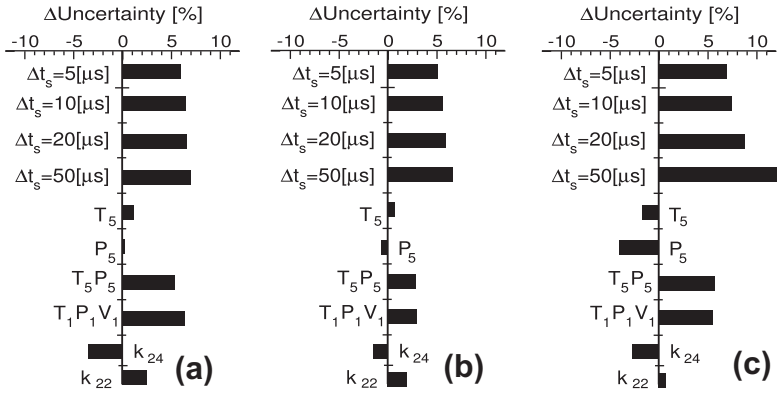

Fig. 12. Sensitivity analyses of the uncertainties in k_1 against "irreducible" uncertainties at three different temperatures: (a) 1000 K, (b) 1500 K, and (c) 2000 K.

effect on increasing the uncertainty is to introduce the uncertainties of the measured time-shift and the combined effect of the uncertainties of T_5 and P_5. On the other hand, the uncertainties of P_5, k_{24}, and k_{22} indeed decrease the uncertainty in k_1 at a certain temperature. The reason why the uncertainty in k_1 increases when we consider both T_5 and P_5, but not when we individually consider them is related to the assumption that we made during construction of $\mathcal{M}_6$ (T_5 and P_5 are uncorrelated).

We would like to provide further insights by comparing the contribution of different uncertainties on the results obtained for models $\mathcal{M}_4$- $\mathcal{M}_6$. Note there are four types of uncertainties considered in this study: experimental uncertainty and irreducible uncertainty which are both fixed, and parametric uncertainty and uncertainty due to model error (denoted by σ) which are both subject to calibration.

Conditioned on model parameters, the total discrepancy between model predictions and experimental data is given by experimental uncertainty, model error (given by σ), and irreducible uncertainty. Thus, if a specific total discrepancy is required by the model, σ is readjusted during calibration to match that discrepancy in the presence of irreducible uncertainty. This explains the decrease in σ for models that account for irreducible uncertainty, see Fig. 11. For example, the difference between σ in model $\mathcal{M}_1$ and model $\mathcal{M}_4$ is due to the irreducible uncertainty in T_5.

In addition to decreasing σ, the irreducible uncertainty affects the correlation between the model parameters (A, m, Θ). This explains why the sensitivities for $\mathcal{M}_5$ and $\mathcal{M}_6$ are opposite even though the marginals for the parameters and σ for both models are the same, see Figs. 9 and 11. These correlations may induce cancellations in the Arrhenius equation, and as a result a reduction in the uncertainty of k. This is the case when comparing $\mathcal{M}_1$ and $\mathcal{M}_4/\mathcal{M}_5$ which account for uncertainty in T_5/P_5. The irreducible uncertainty induces correlations in the parameters that cancel out in the Arrhenius equation, which explains the negative sensitivities for $\mathcal{M}_4$ and $\mathcal{M}_5$. In the case of $\mathcal{M}_6$, the irreducible uncertainty of both T_5 and P_5 induces correlations in the parameters that increase the uncertainty of k_1 when propagated through the Arrhenius equation. Thus the difference in the sensitivities between $\mathcal{M}_4/\mathcal{M}_5$ and $\mathcal{M}_6$ is due to the difference in the correlation structure between model parameters.

This type of sensitivity analysis provides useful information for improving the accuracy of uncertainty estimation of k_1.

6. Conclusions

In this paper, we have used a Bayesian approach along with experimental data recently obtained by Prof. Hanson's research group at Stanford University to quantify the uncertainty in the rate coefficient of $H + O_2 \rightarrow OH + O$. In the first stage, we have used the manufactured data in order to examine whether the system of interest was correctly posed and whether our methodology was capable of retrieving model parameters as solution of the inverse problem. In the second stage, we have constructed the nine stochastic models depending on different choices of ("irreducible") uncertainties accounted for. The objective was in particular to analyze the sensitivity of the "irreducible" uncertainty parameters on uncertainty of k_1. One of our major observations is that the uncertainty of the measured time-shift can significantly increase the uncertainty. We also observe that to consider the correlation between the temperature and gas does not have appreciable impact on the result of the uncertainty estimation. The proposed method seems to be more accurate than a conventional "deterministic" approach in at least two aspects: it allows for the calibration of several random model parameters with the possibility of evaluating their stochastic dependence (e.g. evaluation of higher moments) and it can rigorously consider a variety of uncertainties involved in the calibration process.

Acknowledgement

This material is based upon work supported by the Department of Energy [National Nuclear Security Administration] under Award Number [DE-FC52–08NA28615].

References

[1] M. Panesi, K. Miki, S. Prudhomme, A. Brandis, Computer Methods in Applied Mechanics and Engineering 213 (2011) 383–398.
[2] T. Turányi, T. Nagy, I. Gy Zsély, M. Cserháti, T. Varga, B. Szabó, I. Sedyó, P.T. Kiss, A. Zempléni, H.J. Curran, International Journal of Chemical Kinetics 44 (2012) 284–302.
[3] Z. Hong, D.E. Davidson, E.A. Barbour, R.K. Hanson, Proceedings of the Combustion Institute 33 (2010) 309–316.
[4] J.A. Manion, R.E. Huie, R.D. Levin, D.R. Burgess Jr., V.L. Orkin, W. Tsang, W.S. McGivern, J.W. Hudgens, V.D. Knyazev, D.B. Atkinson, E. Chai, A.M. Tereza, C.-Y. Lin, T.C. Allison, W.G. Mallard, F. Westley, J.T. Herron, R.F. Hampson, D.H. Frizzell, NIST chemical kinetics database, NIST standard reference database 17, version 7.0 (web version), release 1.4.3, data version 2008.12, National Institute of Standards and Technology, Gaithersburg, Maryland, 20899-8320. <http://kinetics.nist.gov/>.
[5] D.A. Sheen, X. You, H. Wang, T. Lovas, Proceedings of the Combustion Institute 32 (2007) 535–542.
[6] D.A. Sheen, H. Wang, Combustion and Flame 158 (2011) 2358–2374.
[7] T. Russi, A. Packard, R. Feeley, M. Frenklach, The Journal of Physical Chemistry 112 (2008) 2579–2588.
[8] M. Frenklach, A. Packard, P. Seiler, Prediction Uncertainty from Models and Data, Proceedings of the American Control Conference, IEEE, New York, 2002.
[9] T. Nagy, T. Turányi, International Journal of Chemical Kinetics 43 (2011) 359–378.
[10] F. Cailliez, P. Pernot, The Journal of Chemical Physics 134 (2011) 054124.
[11] R.R. Upadhyay, K. Miki, O. Ezekoye, J. Marschall, Experimental Thermal and Fluid Science 35 (2011) 1588–1599.

[12] K. Miki, M. Panesi, E. Prudencio, S. Prudhomme, Physics of Plasmas 19 023507.
[13] K. Miki, S.H. Cheung, E.E. Prudencio, P.L. Varghese, International Journal of Chemical Kinetics (2012) http://dx.doi.org/10.1002/kin.20736.
[14] J.L. Beck, L.S. Katafygiotis, Proceedings of the 1st International Conference on Computational Stochastic Mechanics (1991) 125–136.
[15] J.L. Beck, L.S. Katafygiotis, ASCE Journal of Engineering Mechanics 124 (1998) 455–461.
[16] D.L. Baulch, C.T. Bowman, C.J. Cobbs, R.A. Cox, T. Just, J.A. Kerr, M.J. Pilling, D. Stocker, J. Troe, W. Tsang, R. Walker, J. Warnatz, Journal of Physical and Chemical Reference Data 34 (2005) 757–1397.
[17] S.H. Cheung, J.L. Beck, Computer-Aided Civil and Infrastructure Engineerinig 25 (2010) 304–321.
[18] G.P. Smith, D.M. Golden, M. Frenklach, N.W. Moriarty, B. Eiteneer, M. Goldenberg, C.T. Bowman, R.K. Hanson, S. Song, W.C. Gardiner, Z. Lissianski, V.V. Qin, GRI-Mech 3.0. <http://www.me.berkeley.edu/grimech>.
[19] Z. Hong, E.A. Barbour, A. Davidson, R.K. Hanson, The Journal of Physical Chemistry 113 (2009) 12919–12925.
[20] K. Miki, M. Panesi, E.E. Prudencio, S. Prudhomme, Journal of Computational Physics 231 (2012) 3871–3886.
[21] J.T. Herbon, Shock Tube Measurements of $CH_3 + O_2$ Kinetics and the Heat of Formation of the OH radical, Report TSD-153 Stanford University, Stanford. <http://thermosciences.stanford.edu/pdf/TSD-153.pdf>.
[22] S.H. Cheung, T.A. Oliver, E.E. Prudencio, S. Prudhomme, R.D. Moser, Reliability Engineering and System Safety 96 (2011) 1137–1149.
[23] A.N. Pirraglia, J.V. Michael, R.B. Sutherland, J. Klemm, The Journal of Physical Chemistry 93 (1989) 282–291.
[24] D.A. Masten, R.K. Hanson, C.T. Bowman, The Journal of Physical Chemistry 91 (1990) 7119–7128.
[25] M. Conaire, H.J. Curran, J.M. Simmie, W.J. Pitz, C.K. Westbrook, International Journal of Chemical Kinetics 36 (2004) 603–622.
[26] A.E. Lutz, R.J. Kee, J.A. Miller, A Fortran Program for Predicting Homogeneous Gas Phase Chemical Kinetics with Sensitivity Analysis, Report No. sand87-8248, Sandia National Laboratory.
[27] T. Yuan, C. Wang, C. Yu, M. Frenklach, M. Rabinowitz, The Journal of Chemical Physics 95 (1991) 1258–1265.
[28] K.S. Fujii, N. Shin, Chemical Physics Letters 151 (1988) 461–465.
[29] P. Frank, T. Just, Berichte der Bunsen-Gesellschaft für Physikalische Chemie 89 (1985) 181–187.
[30] M.A. Namoradze, A.F. Troshin, V.V. Azatyan, Z.G. Dzotsenidze, M.D. Museridze, Soobshcheniya Akademii Nauk Gruzinskoj SSR 73 (1974) 377–379.
[31] J.A. Miller, B.C. Garrett, International Journal of Chemical Kinetics 29 (1997) 275–287.
[32] T.C. Germann, W.H. Miller, The Journal of Chemical Physics 101 (1997) 6358–6367.